DEPT. OF MATH., UNIVERSITY OF OSLO
RESEARCH REPORT IN MECHANICS, No. 2
ISSN 0801-9940 September 2014

SEMI-ANALYTICAL MODEL FOR COMPRESSIVE STRENGTH ANALYSIS OF IMPERFECT, LONG COMPOSITE PLATES

by

Qiao Jie Yang

Mechanics Division, Department of Mathematics
University of Oslo, Norway

Abstract: A semi-analytical model for ultimate strength prediction of simply supported, rectangular, composite plates has been presented previously. The model is based on large deflection theory in combination with first order shear deformation theory. After damage initiation, a linear degradation of material properties is applied. Rather than dividing the plate into many small elements, as in a finite element analysis, a simplified approach is used in which the plate is divided into nine regions and degradation is confined to the affected region of a failed ply. In the previous work, the model was successfully applied to square plates with an initial geometric imperfection in a single half sine-wave shape, but in the current report an attempt is made to apply it to long plates with mixed modes of geometric imperfections. The strengths estimated for thicker plates are satisfactory, while the predicted strengths for thinner plates are very conservative. It is believed that the division of the plates has significant influence on the strength predictions. In order to obtain more accurate results, alternative locations of the boundaries between ply regions or increasing the number of ply regions should be considered.

Keywords: Composite plate; Ultimate strength; Post-buckling; Linear material degradation; Geometric imperfection.

CONTENTS

1 INTRODUCTION

The application of composites consisting of fibre-reinforced plastics (FRP) is constantly increasing due to their favourable strength-weight ratio. Composite plates are commonly used in many structures, for instance in aircraft, naval ships and wind turbine blades. One subcomponent that is of practical importance in structural design is the long, rectangular laminated plate. Such plates for instance commonly appear in the wing structures of aircraft and in longitudinally stiffened ship hulls (Fig. 1). Numerous types of laminates can be obtained by varying the fibre orientations, number of plies and stacking sequence. Initially, the buckling analysis of composite plates subjected to in-plane loadings has been confined to the determination of elastic buckling loads. This type of analysis generally considered perfectly flat panels, and numerous analytical and numerical approaches are already presented in the literature. Leissa [1] determined the elastic buckling loads of composite panels by using eigenvalue analysis. Such analytical solutions are also adopted by Brunelle and Oyibo [2] for presenting generic buckling curves for specially orthotropic rectangular composite plates. The work by Nemeth [3] concerned the buckling analysis of anisotropic plates with application in spacecraft. The plates were assumed to be long and symmetric, and subjected to combined loads. Non-dimensional buckling design curves were established for both simply supported and clamped boundary conditions. In the design of composite plates, a separate check for material failure is usually performed in addition to the elastic buckling load. For this, local laminate strength data could be used or, alternatively, appropriate failure criteria could be applied at ply level. For many plates, because they exhibit stable post-buckling behaviour, the in-plane load bearing capacity can be much higher than the elastic buckling load. On the other hand, the presence of initial geometric imperfections, often arising from the manufacturing process, tends to reduce the load carrying capacity. In the case of long plates, the situation is more complicated due to the presence of several possible modes of initial geometric imperfections. The imperfection caused by the fabrication can often be approximated by a single sine-waveform while the preferred buckling mode may be another. These effects should be taken into account in order to prevent unsafe predictions.

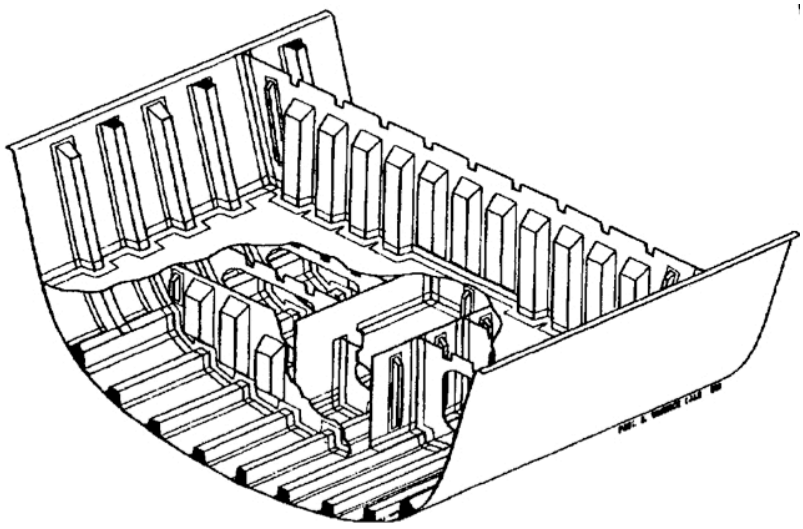

Fig. 1. Longitudinally stiffened composite ship hull structure: Royal Navy Sandown Class minehunter [4].

More recently, in order to increase the full utilisation of composite materials and obtain a more accurate analysis of composite plates, ultimate strength analysis has been introduced that can take account of post-buckling deformations, initial geometric imperfections and progressive material damage. This type of analysis is already available in some finite element (FE) tools and has been reported in several publications. The studies presented in [5] (with application in aircraft) and [6] (with application in marine structures and wind turbine blades) aim to develop a more accurate prediction of collapse for composite panels using FE tools such as ABAQUS. These investigations include progressive failure modelling and also involve the design and testing of panels for validation. However, such advanced nonlinear FE analysis for composites requires special expertise and is normally time consuming in terms of model generation, numerical computation and post-processing. Thus, in many design situations, such advanced FE analysis is impractical, and simplified yet reliable approaches are needed.

Lately, use of semi-analytical methods has become common for strength and buckling analysis of both metal and composite panels. An analytical formulation for the study of local skin buckling and post-buckling of stiffened laminated panels is presented in [7]. In [8], a combination of finite element solution and semi-analytical approach is used for the analysis of laminated composite plates. To the authors' knowledge, the first attempt at including progressive damage modelling in a semi-analytical approach is that described in [9]. The model is an extension of the already available semi-analytical models adopted by Det Norske Veritas Germanischer Lloyd (DNV GL) applied to stiffened/unstiffened steel plates and implemented in the computerised software code PULS for use in the strength assessment of steel ship structures. These models are reported by Steen [10] and Brubak *et al.* [11]. For the strength prediction of laminated composite plates, the present method takes account of post-buckling deformations, initial geometric imperfection, out-of-plane shear deformation and material degradation for composites. Previously [9,12], the investigation has been performed for square composite plates using the analytical and semi-analytical methods. The present report investigates the extent to which the model presented in [9] can be applied to long plates having a mixed mode of imperfections. The Hashin and Rotem failure criterion [13] will be used to detect the failure in the laminates and the material stiffness reduction is confined to the affected region of a failed ply. To validate the method, the numerical results are compared to the nonlinear analysis performed in ABAQUS by Misirlis and reported by Hayman *et al.* in [6].

2 BOUNDARY CONDITIONS AND DISPLACEMENT FIELD

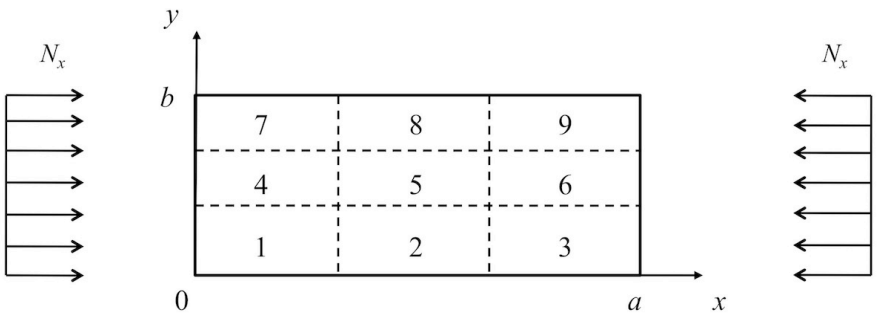

Fig 2. Plate geometry and load condition.

Following [9], a rectangular plate is considered, with dimensions $a \times b$ (Fig. 2) and an initial out-of-plane deformation w_{init}. The plate is simply supported on all edges and subjected to a mean compression N_x in the x-direction. In the analyses, this is achieved by restraining the edge $x = 0$ in the x-direction and applying a uniform, negative displacement u_c in the x-direction on the edge $x = a$, all four edges being held straight. The total out-of-plane deformation is $w_{tot}=w_{init}+w$. The adopted displacement field is given in Eqs. (1), and each deformation component is assumed in the form of a truncated double Fourier series [14], the in-plane displacements having in addition a linear component [11,15]:

$$u_0(x,y) = \sum_{n=1}^{N}\sum_{m=1}^{M} u_{mn} \sin\left(\frac{m\pi x}{a}\right)\cos\left(\frac{n\pi y}{b}\right) + u_c \frac{x}{a} \tag{1a}$$

$$v_0(x,y) = \sum_{n=1}^{N}\sum_{m=1}^{M} v_{mn} \cos\left(\frac{m\pi x}{a}\right)\sin\left(\frac{n\pi y}{b}\right) + v_c \frac{y}{b} \tag{1b}$$

$$\phi_x(x,y) = \sum_{n=1}^{N}\sum_{m=1}^{M} x_{mn} \cos\left(\frac{m\pi x}{a}\right)\sin\left(\frac{n\pi y}{b}\right) \tag{1c}$$

$$\phi_y(x,y) = \sum_{n=1}^{N}\sum_{m=1}^{M} y_{mn} \sin\left(\frac{m\pi x}{a}\right)\cos\left(\frac{n\pi y}{b}\right) \tag{1d}$$

$$\begin{aligned} w_{tot}(x,y) &= w(x,y) + w_{init}(x,y) \\ &= \sum_{n=1}^{N}\sum_{m=1}^{M} w_{mn} \sin\left(\frac{m\pi x}{a}\right)\sin\left(\frac{n\pi y}{b}\right) + \sum_{n=1}^{N}\sum_{m=1}^{M} w_{imn} \sin\left(\frac{m\pi x}{a}\right)\sin\left(\frac{n\pi y}{b}\right) \end{aligned} \tag{1e}$$

The symbols u_0 and v_0 represent the mid-plane displacements in the x- and y-directions, respectively. The rotations of a transverse normal about axes parallel to the y and x axes are denoted by ϕ_x and ϕ_y, respectively. The coefficients u_c, v_c, u_{mn}, v_{mn}, x_{mn}, y_{mn} and w_{mn} are unknowns, w_{imn} are given imperfection amplitudes, and m, n, M and N are positive integers.

3 METHODOLOGY

The semi-analytical method is based on large deflection bending theory combined with the first order shear deformation theory. The load-displacement response is traced by an incremental procedure, where an arc length parameter is used as a propagation parameter [10]. This method is presented in detail in Yang [9] and the Riks-Wempner iterative procedure [16,17] is applied within each load increment to correct for the disagreement between the external applied forces and the internal forces. As in [9], a convergence criterion is introduced to determine the number of iterations needed within each load step. This criterion is based on the magnitudes of the unbalanced forces U and the internal forces I [18]:

$$\|U\| < \beta\|I\| \tag{2}$$

In the analyses performed in Section 6, the chosen value of β is set to 0.01.

4 PROGRESSIVE FAILURE MODELS

4.1 Hashin and Rotem Failure Criterion

The Hashin and Rotem failure criterion for in-plane stresses can be written [13]:

$$f_1^T = \left(\frac{\sigma_{11}}{X_t}\right)^2 = 1 \;;\; f_2^T = \left(\frac{\sigma_{22}}{Y_t}\right)^2 + \left(\frac{\tau_{12}}{S_{12}}\right)^2 = 1 \tag{3a}$$

$$f_1^C = \left(\frac{\sigma_{11}}{X_c}\right)^2 = 1 \;;\; f_2^C = \left(\frac{\sigma_{22}}{Y_c}\right)^2 + \left(\frac{\tau_{12}}{S_{12}}\right)^2 = 1 \tag{3b}$$

Failure occurs when any of the four failure functions from Eqs. (3) reaches unity. Each is associated with a dominant failure mode.

4.2 Degradation of Properties

A damaged material stiffness matrix for in-plane deformations is defined [6]:

$$[R] = \begin{bmatrix} (1-d_1)R_{11} & (1-d_1)(1-d_2)R_{12} & 0 \\ sym. & (1-d_2)R_{22} & 0 \\ sym. & sym. & (1-d_6)R_{66} \end{bmatrix} \tag{4}$$

Here d_1 is the damage factor for the longitudinal direction of the material, d_2 is that for the transverse direction, and d_6 is that for the in-plane shear component. The remaining parameters in Eq. (4) are defined as $R_{11} = \frac{E_1}{\Delta}$, $R_{22} = \frac{E_2}{\Delta}$, $R_{12} = \frac{\nu_{12}E_2}{\Delta}$, $R_{66} = G_{12}$ and $\Delta = 1 - \nu_{12}\nu_{21}(1-d_1)(1-d_2)$.

For the Hashin and Rotem criterion, because the shear failure component is associated with both fibre and matrix modes of failure, the damage variable d_6 is defined as:

$$d_6 = 1 - (1-d_1)(1-d_2) \tag{5}$$

To allow direct comparison with the results of Misirlis [6], the transverse (out-of-plane) shear stiffness matrix is not degraded during the analysis. (The ABAQUS shell elements used by Misirlis did not allow such degradation) Thus

$$[K] = \begin{bmatrix} K_{44} & 0 \\ 0 & K_{55} \end{bmatrix} \tag{6}$$

where $K_{44} = G_{23}$ and $K_{55} = G_{13}$.

4.3 Material Degradation

For the linear degradation of the material properties, as used in the present work, the degradation procedure is based on the constitutive model proposed by Matzenmiller *et al.* [19], i.e. the damage evolution is similar to the model implemented in ABAQUS. More information is given in Appendix A [20].

5 PLY REGION DEGRADATION MODEL (PRDM)

To use the ply region degradation model (PRDM), first introduced in [12], the plate is divided into 9 regions as shown by the broken lines in Fig. 1. Thus regions 1, 3, 7 and 9 are corner regions, 5 is a centre region and 2, 4, 6 and 8 are mid-edge regions (of which 4 and 6 are loaded edges). This division was first introduced for square plates with a half sine-waveform buckling mode to enable differentiation between regions having differing predominant stress states. The procedure implemented with linear material degradation and the Riks-Wempner method is presented in Fig. 3.

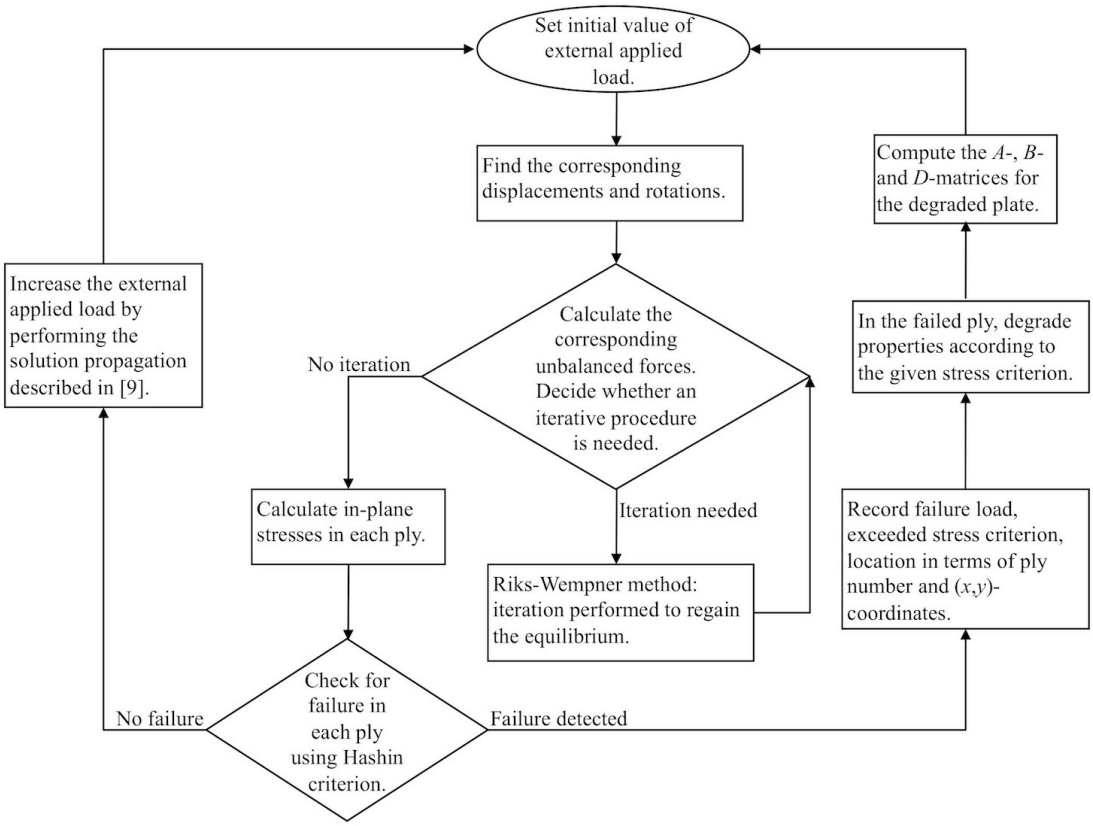

Fig. 3. Schematic diagram: the procedure using PRDM with the linear material degradation. The procedure is repeated until the maximum load is reached.

6 PARAMETRIC STUDY

6.1 Description

To test the simplified approach by comparing results with those obtained by Misirlis using advanced FE analysis [6], parametric studies have been performed for a series of long plates, with a = 2000 mm and b = 500 mm, having various b/t ratios and initial imperfection amplitudes 0.1%, 1% and 3% of the width b. The shape of the initial geometric imperfection is a combination of 20% of the preferred buckling mode shape and 80% of a single half sine wave. Two different types of composite layup are considered [6]:

- Case A, a triaxial layup: $\left[-45 / +45 / 0_4 / +45 / -45 / 0_4 / -45 / +45 / 0_3\right]_S$
  This layup configuration is typical for the main spar of a wind turbine blade.
- Case B, a quasi-isotropic, quadriaxial layup: $\left[0 / +45 / 90 / -45\right]_{X,S}$
  This layup configuration is more typical for ship hull panels that experience a mixture of lateral pressure and in-plane loading due to hull girder bending.

A so-called plate affine aspect ratio is introduced in [2] for determining the preferred buckling mode and establishing generic buckling curves for specially orthotropic plates. This is defined as

$$\frac{a_0}{b_0} = \left(\frac{D_{22}}{D_{11}}\right)^{1/4} \frac{a}{b} \tag{7}$$

Here, a_0/b_0 is the plate affine aspect ratio, and D_{11} and D_{22} are the terms in the bending stiffness matrix corresponding to bending in the x- and y-directions. For simply supported, specially orthotropic plates, Brunelle and Oyibo derived the generic buckling curves shown in Fig. 4. This figure also shows the transitions between regions with differing preferred buckling modes. In Fig. 4, the affine plate buckling coefficient is given by k_0 and D^* is the generalised rigidity ratio. These are given in Eqs. (8).

$$k_0 = \frac{N_x b^2}{\pi^2 \sqrt{D_{11} D_{22}}} \tag{8a}$$

$$D^* = \frac{D_{12} + 2D_{66}}{\sqrt{D_{11} D_{22}}} \tag{8b}$$

Here, D_{12} and D_{66} are the in-plane bending coupling term and the twisting term in the bending stiffness matrix, respectively.

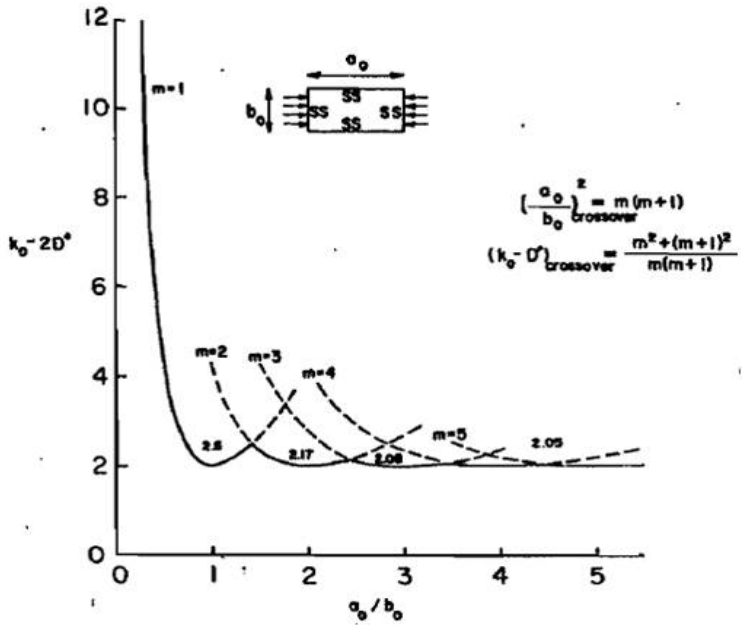

Fig.4. Modified uniaxial buckling coefficients vs affine aspect ratio for simply supported (SS) boundary conditions provided by Brunelle and Oyibo [2]. Here *m* is the number of half-waves in the longitudinal direction.

For the layup case A with $a/b = 4$, $D_{22}/D_{11} \approx 0.38$, which implies $a_0/b_0 \approx 3.14$. Thus, the preferred buckling mode for layup case A is three half-sine waves ($m = 3$). For the layup case B, the plate affine aspect ratio is in the range 3.48-3.92, depending on the number of plies. Thus, the preferred buckling mode for the layup case B is four half-sine waves ($m = 4$). The initial geometric imperfections are presented in Eqs. (9) with the imperfection amplitude $\bar{w}_i$. The coefficients 1.403 and 1.052 are included in the equations for the layup cases A and B, respectively, thus the maximum combined amplitude in each layup case is equal to the given imperfection amplitude.

$$w_{init,\mathrm{A}}(x,y) = 1.403 \cdot \bar{w}_i \sin\left(\frac{\pi y}{b}\right)\left(0.80 \cdot \sin\left(\frac{\pi x}{a}\right) + 0.20 \cdot \sin\left(\frac{3\pi x}{a}\right)\right) \tag{9a}$$

$$w_{init,\mathrm{B}}(x,y) = 1.052 \cdot \bar{w}_i \sin\left(\frac{\pi y}{b}\right)\left(0.80 \cdot \sin\left(\frac{\pi x}{a}\right) + 0.20 \cdot \sin\left(\frac{4\pi x}{a}\right)\right) \tag{9b}$$

Following Misirlis [6], for the triaxial layups (case A), the required b/t values are achieved by scaling the thickness of each individual ply. For the quadriaxial layups (case B), the thickness is increased by adding groups of plies (increasing X) to give the desired b/t values. The material properties and the plate thicknesses for cases A and B are given in Tables 1-2. Note that ply number 1 is located on the concave side of the plate when the imperfection component with $m = 1$ is applied. For the ply region degradation model (see Fig. 1), regions 1, 3, 7 and 9 are each 650 mm × 160 mm, regions 2 and 8 are each 700 mm × 160 mm, regions 4 and 6 are 650 mm × 180 mm and region 5 is 700 mm × 180 mm.

Table 1
Material properties (strengths and moduli).

Property	E_1	E_2	ν_{12}	G_{12}	G_{13}	G_{23}	X_t	X_c	Y_t	Y_c	S_{12}
Value	49627	15430	0.272	4800	4800	4800	968	915	24	118	65
Units	MPa	MPa	-	MPa	MPa	MPa	MPa	MPa	MPa	MPa	MPa

Table 2
Plate thicknesses and ply thicknesses for case A layups (left) and case B layups (right).

Layup	b/t	t (mm)	t_0 (mm)	$t_{\pm 45}$ (mm)	Layup	b/t	t (mm)	X	t_0, $t_{\pm 45}$, t_{90} (mm)
A1	50	10.02	0.39	0.12	B1	62.50	8.00	1	1.00
A2	30	16.70	0.65	0.20	B2	31.25	16.00	2	1.00
A3	20	24.94	0.97	0.30	B3	20.83	24.00	3	1.00
A4	15	33.40	1.30	0.40	B4	15.63	32.00	4	1.00
A5	10	49.98	1.95	0.59	B5	10.42	48.00	6	1.00

6.2 Load-displacement Response Without Material Degradation

The load-end shortening responses for the layup cases A1 and B1 in Table 2 with 3% imperfection are provided in Fig.5. In the case of long plates with the combined modes of geometric imperfections, the change in the deformation shape for the thin plate sometimes occurs with a snap-back behaviour that is visible in Fig.5. For the layup cases A1 and B1, the change of the buckling modes occurred at approximately 70 MPa and 35 MPa, respectively. This figure is included to demonstrate that the geometrically nonlinear formulation is fully capable of reproducing such behaviour.

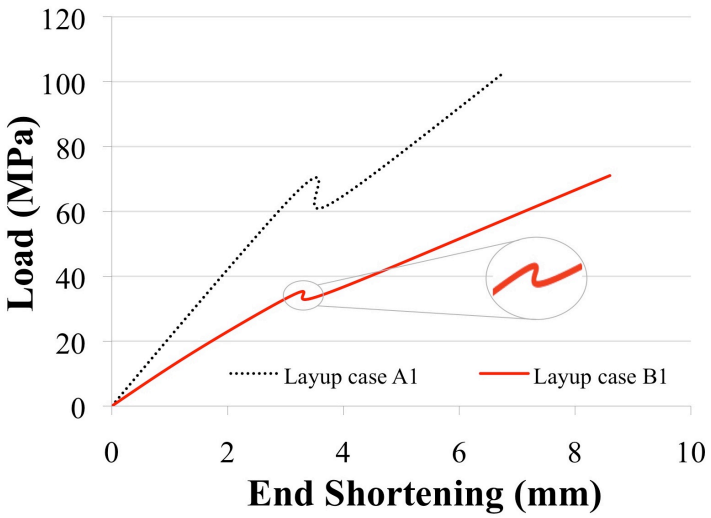

Fig 5. Load vs. end shortening for the layup cases A1 and B1 with 3% imperfection amplitude.

6.3 Ultimate Strength Predictions

The detailed results using the present method are given in Appendix B, Tables B.1-B.2 for cases A and B, respectively. In Figs. 6 and 9, the ultimate strength for a range of b/t values is presented along with the corresponding results presented by Misirlis. The ratios of the ultimate strengths estimated using the present model to the reference values

found by Misirlis are shown in Figs. 7 and 10 for various values of plate thickness t and imperfection amplitude.

For the triaxial layup, case A, the shapes of the graphs provided in Fig. 6 are somewhat similar to those of Misirlis with some exceptions, which are also indicated in Fig. 7: the results estimated for the layup case A2 are better than layup case A3 with imperfections 0.1% and 1%. The predicted strengths are in the range of 10% higher to 51% lower compared to the ABAQUS results. The best results are obtained for the thicker plates, i.e. the layup cases A4 and A5 in Table 2, and the greatest discrepancies are observed for the layup case A1. Figure 8 shows the deformed shape of the plate after the ultimate load is reached for layup case A5 with 3% imperfection.

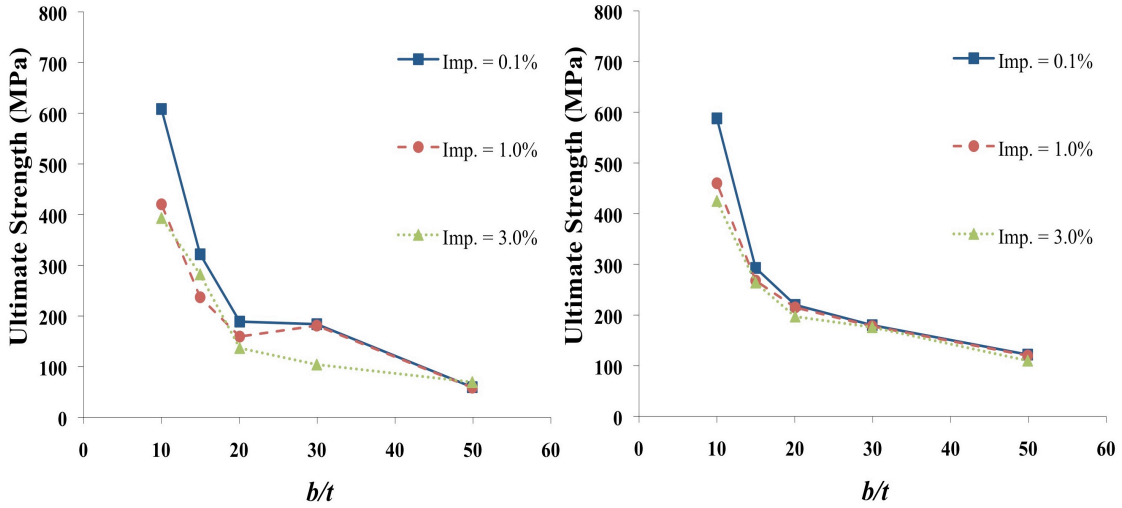

Fig. 6. Case A (triaxial layup): the ultimate strengths from the present analyses (left) are compared to the corresponding results obtained by Misirlis (right) [6] for various b/t values and imperfection amplitudes.

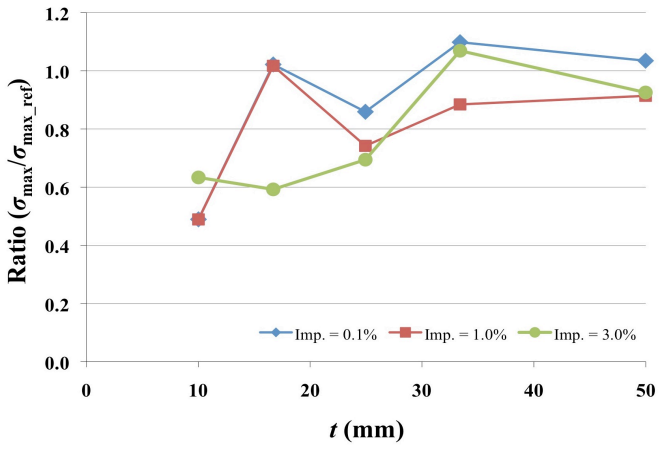

Fig. 7. Case A (triaxial layup) with PRDM: the ultimate strengths from the present analyses are compared to the reference values σ_{max_ref} obtained by Misirlis, for various plate thicknesses t and imperfection amplitudes.

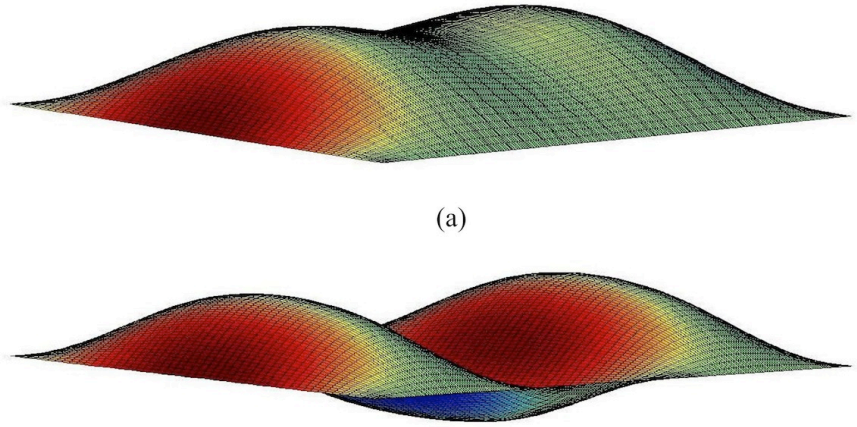

Fig. 8. Layup case A5 with 3% imperfection: the plate shape with the initial geometric imperfection (a) and the deformed shape of the plate after the ultimate load is reached (b).

For the quadriaxial layup, case B, the shapes of the graphs provided in Fig. 9 are slightly different compared to those of Misirlis, and this is mainly related to the layup cases B2 and B3. The estimated strengths are in the range 3% - 68% lower than ABAQUS results. The best results are achieved for the thicker plates, i.e. the layup cases B4 and B5 in Table 2, and the greatest discrepancies are observed for the layup case B1. In contrast to the layup case A, a trend is observed here: the agreement with the ABAQUS prediction increases with the plate thickness. Figure 11 shows the deformed shape of the plate after the ultimate load is reached for layup case B2 with 1% imperfection.

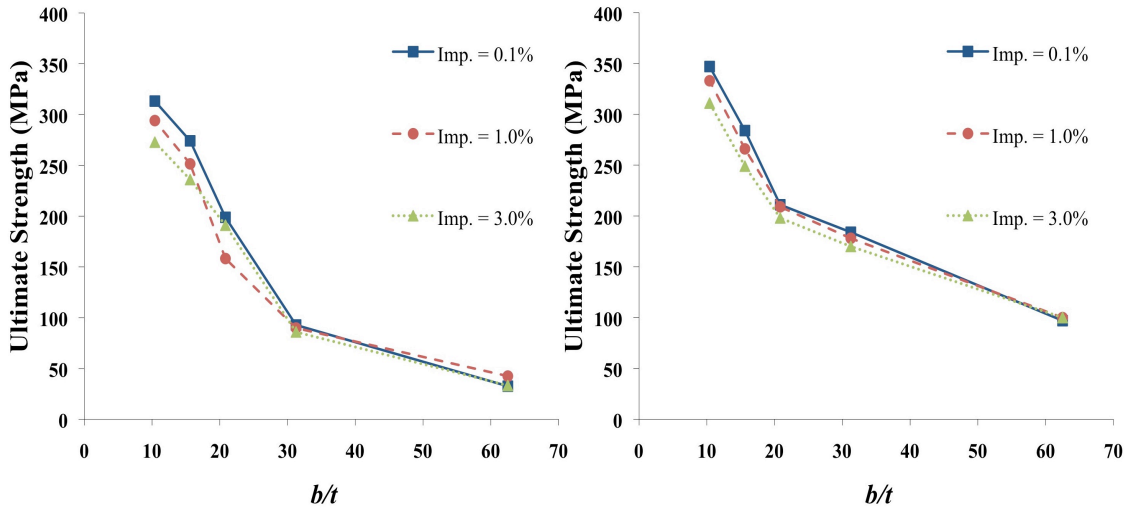

Fig. 9. Case B (quadriaxial layup): the ultimate strengths from the present analyses (left) are compared to the corresponding results obtained by Misirlis (right) [6] for various *b*/*t* values and imperfection amplitudes.

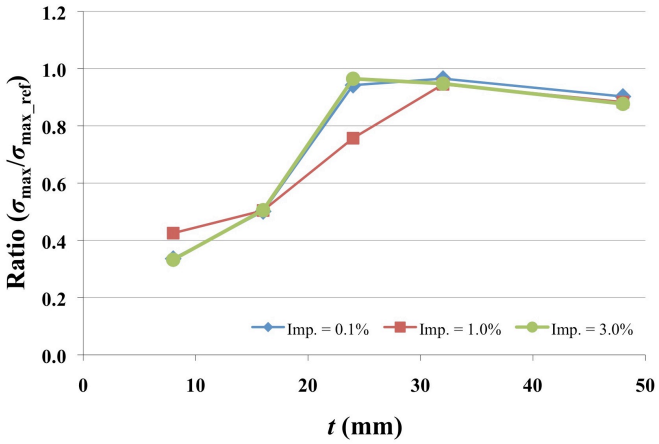

Fig. 10. Case B (quadriaxial layup) with PRDM: the ultimate strengths from the present analyses are compared to the reference values σ_{max_ref} obtained by Misirlis, for various plate thicknesses t and imperfection amplitudes.

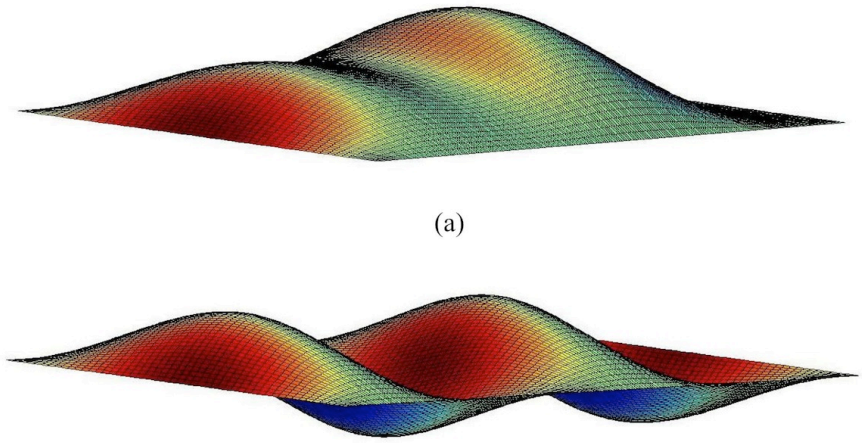

(a)

(b)

Fig. 11. Layup case B2 with 1% imperfection: the plate shape with the initial geometric imperfection (a) and the deformed shape of the plate after the ultimate load is reached (b).

7 DISCUSSION

To improve computational efficiency, Misirlis modelled only half of the panel in ABAQUS and imposed symmetry boundary conditions at the edge corresponding to the longitudinal centre-line. This may have caused some inaccuracies since composite plates do not necessarily degrade symmetrically. However, the error introduced by this approximation is not expected to be significant.

For long plates, the ultimate strengths predicted using the present model are acceptable for the thicker plates, while for the thinner plates the predictions are clearly too conservative. This could be explained by the fact that the long plates have been divided into 9 regions as in [9,12]. In the earlier studies on square plates, the thinner plates, characterised by small ply thicknesses (case A) and few plies (case B), were found to be the most sensitive to the plate division [9]. The present ply region based

material degradation appears to result in unnecessarily large stiffness-reduced areas. The total plate stiffness can thus be significantly affected for these plates, even with a small number of regions damaged. This will in turn provide incorrect stress distribution throughout the plate. Especially for the layup case B1 with 8 plies only, it seems that there is almost no reserve strength beyond first ply failure. For the layup case A1, the situation is slightly better since this has 34 plies. Furthermore, as the load increases, the shape of the plate deformation follows the preferred buckling mode shape, and it is suspected that the change of the buckling modes during the analysis causes more difficulty for the progressive failure model. Once a ply region fulfils the failure criterion in one buckling mode, the material stiffness degradation is initiated based on the single equivalent strain value (δ_{eq}^{0}) for this ply region and this dominates throughout the degradation process. This value could be correct to a certain point of the analysis, but also randomly too rough to give a true picture of the degradation process: the ply region may consist of an area that should undergo either more or less stiffness reduction as one buckling mode takes over from another. This is believed to affect both thin and thick plates, but especially for thinner plates the influence is significant. In contrast, Misirlis performed the ABAQUS analysis with the element size 20 mm × 20 mm. However, the thick plates are less sensitive to the plate division since these plates undergo less bending deformation than thinner plates, so that stresses are more uniformly distributed throughout the plate.

In order to improve the PRDM for estimating more accurate ultimate strengths for long plates, alternative locations of the boundaries between ply regions should be considered or the total number of the ply regions should be increased. From the previous work [9], it is shown that the strength predictions based on this PRDM with 9 regions are satisfactory for square plates (aspect ration $a/b = 1$) having a half-sine waveform imperfection. It seems that this plate division remains correct as long as the buckling mode maintains a half-sine waveform. According to [2], this is possible if the affine aspect ratio $a_0/b_0 < 1.41$, which results in the actual aspect ratio $a/b < 1.78$ for the layup case A and approximately $a/b < 1.50$ for the layup case B. Since the shape of the plate deformation follows the preferred buckling mode shape, the number of the ply regions could be determined based on that. Previously in [9], 3 regions in the axial direction were found to provide satisfactory results for the square plate with a half sine-wave buckling shape. Theoretically, for long plates having the aspect ratio equal to 4, it is likely that the PRDM should be implemented with approximately 27 and 36 ply regions for the layup cases A (three half sine-waveform deformation shape) and B (four half sine-waveform deformation shape), respectively. However, this assertion has not been pursued in the present study.

8 CONCLUSIONS

Ultimate strength prediction using a semi-analytical method has been studied for simply supported, long composite plates subjected to uniaxial in-plane compressive load. The present model takes account of post-buckling deformations, out-of-plane shear deformations and mixed modes of initial geometric imperfections. The plate has been divided into nine regions and the linear material stiffness degradation has been applied to the failed region in a ply. A parametric study has been performed for long plates with the aspect ratio $a/b = 4$ having a range of thicknesses and geometric

imperfections. The numerical results have been compared with the FE analysis performed by Misirlis [6]. The strength predictions obtained are satisfactory for thicker plates. For thinner plates, the ultimate strengths are conservatively estimated. This could be explained by fact that the plates have been divided into 9 regions as for square plates in [9,12], and such division of long plates appears to cause a stiffness reduction over an unnecessarily large area, and in turn the stresses are not correctly distributed throughout the plate after damage initiation. In contrast, thick plates undergo less bending deformation than thinner plates, so that stresses are more uniformly distributed throughout the plate. The present nine-region based degradation model is applicable for plates having an affine aspect ratio $a_0/b_0 < 1.41$, which provides a single sine-waveform buckling mode. This in turn gives the actually aspect ratio $a/b < 1.78$ for the layup case A and approximately $a/b < 1.50$ for the layup case B. For higher aspect ratios, other locations of the ply region boundaries or increasing the number of ply regions should be considered in order to provide more accurate strength prediction.

ACKNOWLEDGEMENTS

The author wishes to thank Professor Brian Hayman at the University of Oslo for his constructive advice and valuable discussions during the development of this research work.

RERERENCES

[1] Leissa AW. Buckling of laminated composite plates and shell panels. Flight Dynamics Laboratory Report No. AFWAL-TR-85-3069. USA: The Ohio State University, Wright-Patterson Air Force Base; 1985.

[2] Brunelle EJ, Oyibo GA. Generic buckling curves for specially orthotropic rectangular plates. AIAA J 1983;21(8):1150-1156.

[3] Nemeth MP. Buckling behaviour of long anisotropic plates subjected to combined loads. NASA Technical Paper 3568, USA; 1995.

[4] Smith CS. Design of marine structures in composite materials. Elsevier Applied Science; 1990

[5] Orifici AC, Thomson RS, Degenhardt R, Kling A, Rohwer K, Bayandor J. Degradation investigation in a postbuckling composite stiffened fuselage panel. Compos Struct, 2008;82(2):217-224.

[6] Hayman B, Berggreen C, Lundsgaard-Larsen C, Delarche A, Toftegaard H, Dow RS, Downes J, Misirlis K, Tsouvalis N, Douka C. Studies of the buckling of composite plates in compression. Ships Offshore Struct 2011;6(1-2):81-92.

[7] Bisagni C, Vescovini R. Analytical formulation for local buckling and post-buckling analysis of stiffened laminated panels. Thin-walled Struct 2009;47(3):318-334.

[8] Sheng HY, Ye JQ. A semi-analytical finite element for laminated composite plates. Compos Struct, 2002;57:117-123.

[9] Yang QJ. Post-buckling and ultimate strength prediction of composite plates using a semi-analytical method. Research Report in Mechanics. Norway: University of Oslo; 2013 (revised 2014). https://www.duo.uio.no/bitstream/handle/10852/39237/revidert-Researchrep2.pdf

[10] Steen E. Application of the perturbation method to plate buckling problems. Research Report in Mechanics No. 98-1. Norway: University of Oslo; 1998.

[11] Brubak L, Hellesland J. Semi-analytical postbuckling analysis of stiffened imperfect plates with a free or stiffened edge. Comput Struct 2011;89(17-18):1574-1585.

[12] Yang QJ, Hayman B, Osnes H. Trials with a simplified method for buckling and ultimate strength analysis of composite plates. Research Report in Mechanics. Norway: University of Oslo; 2012 (revised 2014). https://www.duo.uio.no/bitstream/handle/10852/39357/revidert-Researchrep1.pdf

[13] Hashin Z, Rotem A. A fatigue failure criterion for fiber reinforced materials. J Compos Mater 1973;7:448-464.

[14] Reddy JN. Mechanics of laminated composite plates and shells. 2nd ed. USA: CRC Press; 2004.

[15] Bažant ZP, Cedolin L. Stability of structures. USA: Oxford University Press; 1991.

[16] Riks E. An incremental approach to the solution of snapping and buckling problems. Int J Solids Struct 1979;15:529-551.

[17] Wempner GA. Discrete approximations related to nonlinear theories of solids. Int J Solids Struct 1971;7:1581-1599.

[18] Crisfield MA. Non-linear finite element analysis of solids and structures. Vol. 1. England: Wiley; 1991.

[19] Matzenmiller A, Lubliner J, Taylor RL. A constitutive model for anisotropic damage in fiber-composites. Mech Mater 1995;20(2):125-152.

[20] Abaqus Documentation. Version 6.11. USA: Dassault Systèms Simulia Corporation; 2011.

APPENDIX A: DAMAGE EVOLUTION AND FAILURE

Equivalent stress (σ_{eq}) and strain (δ_{eq}) for each of the four damage modes are defined as follows:

- Fibre tension:

$$\delta_{eq}^{ft} = \langle \varepsilon_{11} \rangle \quad , \quad \sigma_{eq}^{ft} = \frac{\langle \sigma_{11} \rangle \langle \varepsilon_{11} \rangle}{\delta_{eq}^{ft}} = \langle \sigma_{11} \rangle \tag{A.1}$$

- Fibre compression:

$$\delta_{eq}^{fc} = \langle -\varepsilon_{11} \rangle \quad , \quad \sigma_{eq}^{fc} = \frac{\langle -\sigma_{11} \rangle \langle -\varepsilon_{11} \rangle}{\delta_{eq}^{fc}} = \langle -\sigma_{11} \rangle \tag{A.2}$$

- Matrix tension:

$$\delta_{eq}^{mt} = \sqrt{\langle \varepsilon_{22} \rangle^2 + \gamma_{12}^2} \quad , \quad \sigma_{eq}^{mt} = \frac{\langle \sigma_{22} \rangle \langle \varepsilon_{22} \rangle + \tau_{12}\gamma_{12}}{\delta_{eq}^{mt}} \tag{A.3}$$

- Matrix compression:

$$\delta_{eq}^{mc} = \sqrt{\langle -\varepsilon_{22} \rangle^2 + \gamma_{12}^2} \quad , \quad \sigma_{eq}^{mc} = \frac{\langle -\sigma_{22} \rangle \langle -\varepsilon_{22} \rangle + \tau_{12}\gamma_{12}}{\delta_{eq}^{mc}} \tag{A.4}$$

The symbols $\langle\ \rangle$ in the equations above represent the Macaulay bracket operator which is defined for every $a \in \Re$ as $\langle a \rangle = (a + |a|)/2$. Computation of the damage variables is based on the stress-strain relation shown in Fig. A.1. The positive slope of the stress-strain curve prior to damage initiation corresponds to linear elastic behaviour. After damage initiation, the negative slope is achieved by evolution of the respective damage variables according to the equations (A.1)-(A.4). After damage initiation (i.e. $\delta_{eq} \geq \delta_{eq}^0$), the damage variable d_i for a particular mode is given by

$$d_i = \frac{\delta_{eq}^f \left(\delta_{eq} - \delta_{eq}^0\right)}{\delta_{eq} \left(\delta_{eq}^f - \delta_{eq}^0\right)} \tag{A.5}$$

Here, δ_{eq}^0 representing the strain at which the initiation criterion for the respective mode was met and δ_{eq}^f the strain at which the material is completely damaged in this failure mode. For both matrix and fibre failure modes, $\delta_{eq}^f = \alpha \delta_{eq}^0$ has been used in the cases investigated.

APPENDIX B: TABULATED RESULTS

For a given layup case with a given initial geometric imperfection amplitude, plate thickness (t) and total number of plies (ply regions), Tables B.1-B.2 show the total number of terms included, the $\Delta\eta$ values and the calculated stress (σ_{FPF}) at first ply failure (FPF). The ultimate stress using the semi-analytical method is presented as σ_{max}. The results from the analysis are compared with those obtained by Misirlis (σ_{max_ref}). The ratio of the ultimate strength from the present model to that found by Misirlis are given in the last column ($\sigma_{max}/\sigma_{max\_ref}$).

The numbers of terms used are shown in Tables B.1-B.2; 247 terms to $N = M = 7$ and 407 terms to $N = M = 9$ and 607 terms corresponds to $N = M = 11$. The chosen basic value of N_x is 150 N/mm for layup cases A1 and B1, and 250 N/mm for layup cases A2 and B2. For layup cases A3 and B3, N_x is set to 500 N/mm. For layup cases A4 and B4, N_x is set to 1000 N/mm. The remaining layup cases are implemented with N_x = 2000 N/mm.

Table B.1
Strength predictions for layup case A.

Layup case	Imp. % of b	t (mm)	No. of plies (no. of ply regions)	No. of terms	$\Delta\eta$	σ_{FPF} (MPa)	σ_{max} (MPa)	σ_{max_ref} (MPa)	$\frac{\sigma_{max}}{\sigma_{max\_ref}}$
A1	0.1	10.02	34 (306)	607	0.05	40.71	59.68	122	0.49
A2	0.1	16.70	34 (306)	607	0.10	88.98	183.91	180	1.02
A3	0.1	24.94	34 (306)	407	0.10	185.02	188.98	220	0.86
A4	0.1	33.40	34 (306)	407	0.10	314.48	321.78	293	1.10
A5	0.1	49.98	34 (306)	247	0.10	393.91	608.32	588	1.03
A1	1.0	10.02	34 (306)	607	0.05	37.91	58.67	120	0.49
A2	1.0	16.70	34 (306)	607	0.10	75.63	181.03	178	1.02
A3	1.0	24.94	34 (306)	407	0.10	124.70	159.49	215	0.74
A4	1.0	33.40	34 (306)	407	0.10	178.37	237.00	268	0.88
A5	1.0	49.98	34 (306)	247	0.10	276.93	420.37	460	0.91
A1	3.0	10.02	34 (306)	607	0.05	69.03	69.66	110	0.63
A2	3.0	16.70	34 (306)	607	0.10	75.49	104.23	176	0.59
A3	3.0	24.94	34 (306)	407	0.10	89.64	136.78	197	0.69
A4	3.0	33.40	34 (306)	407	0.10	108.06	282.17	264	1.07
A5	3.0	49.98	34 (306)	247	0.10	146.46	393.28	425	0.93

Table B.2
Strength predictions for layup case B.

Layup case	Imp. % of b	t (mm)	No. of plies (no. of ply regions)	No. of terms	$\Delta\eta$	σ_{FPF} (MPa)	σ_{max} (MPa)	σ_{max_ref} (MPa)	$\frac{\sigma_{max}}{\sigma_{max\_ref}}$
B1	0.1	8.00	8 (72)	607	0.05	32.61	32.61	97	0.34
B2	0.1	16.00	16 (144)	607	0.10	92.19	92.82	184	0.50
B3	0.1	24.00	24 (216)	407	0.10	192.24	198.83	211	0.94
B4	0.1	32.00	32 (288)	407	0.10	206.42	274.11	284	0.97
B5	0.1	48.00	48 (432)	247	0.10	207.85	313.24	347	0.90
B1	1.0	8.00	8 (72)	607	0.05	28.87	42.54	100	0.43
B2	1.0	16.00	16 (144)	607	0.10	77.18	89.81	178	0.50

B3	1.0	24.00	24 (216)	407	0.10	134.05	158.24	209	0.76
B4	1.0	32.00	32 (288)	407	0.10	188.50	251.44	266	0.95
B5	1.0	48.00	48 (432)	247	0.10	198.50	294.05	333	0.88
B1	3.0	8.00	8 (72)	607	0.05	32.58	33.26	100	0.33
B2	3.0	16.00	16 (144)	607	0.10	62.52	85.97	170	0.51
B3	3.0	24.00	24 (216)	407	0.10	91.95	191.02	198	0.96
B4	3.0	32.00	32 (288)	407	0.10	116.44	235.98	249	0.95
B5	3.0	48.00	48 (432)	247	0.10	158.48	272.76	311	0.88